

Targeted optogenetic stimulation of the thalamic reticular nucleus: A novel strategy for modulating epileptiform discharges

Zhi-Hui Wang(王智慧), Jia-Hui Yang(杨佳慧), and Li-Xia Duan(段利霞)
Citation: Chin. Phys. B, 2026, 35 (**6**): 068701. DOI: 10.1088/1674-1056/ae516f
http://cpb.iphy.ac.cn; http://iopscience.iop.org/cpb

What follows is a list of articles you may be interested in

Bifurcation dynamics govern sharp wave ripple generation and rhythmic transitions in hippocampal-cortical memory networks

Xin Jiang(姜鑫), Jialiang Nie(聂嘉良), Denggui Fan(樊登贵), and Lixia Duan(段利霞)
Chin. Phys. B, 2025, 34 (**12**): 128702. DOI: 10.1088/1674-1056/ae111d

Dual mechanisms of Bcl-2 regulation in IP_3-receptor-mediated Ca^{2+} release: A computational study

Hong Qi(祁宏), Zhi-Qiang Shi(史志强), Zhi-Chao Li(李智超), Chang-Jun Sun(孙长君), Shi-Miao Wang(王世苗), Xiang Li(李翔), and Jian-Wei Shuai(帅建伟)
Chin. Phys. B, 2021, 30 (**10**): 108704. DOI: 10.1088/1674-1056/ac1e0d

Dynamics and coherence resonance in a thermosensitive neuron driven by photocurrent

Ying Xu(徐莹), Minghua Liu(刘明华), Zhigang Zhu(朱志刚), Jun Ma(马军)
Chin. Phys. B, 2020, 29 (**9**): 098704. DOI: 10.1088/1674-1056/ab9dee

Generating mechanism of pathological beta oscillations in STN-GPe circuit model: A bifurcation study

Jing-Jing Wang(王静静), Yang Yao(姚洋), Zhi-Wei Gao(高志伟), Xiao-Li Li(李小俚), Jun-Song Wang(王俊松)
Chin. Phys. B, 2020, 29 (**5**): 058701. DOI: 10.1088/1674-1056/ab7e9b

Near equilibrium dynamics and one-dimensional spatial-temporal structures of polar active liquid crystals

Yang Xiao-Gang (杨小刚), M. Gregory Forest, Wang Qi (王奇)
Chin. Phys. B, 2014, 23 (**11**): 118701. DOI: 10.1088/1674-1056/23/11/118701

SPECIAL TOPIC — Biophysical circuits: Modeling & applications in neuroscience

Targeted optogenetic stimulation of the thalamic reticular nucleus: A novel strategy for modulating epileptiform discharges

Zhi-Hui Wang(王智慧), Jia-Hui Yang(杨佳慧), and Li-Xia Duan(段利霞)[†]

College of Science, North China University of Technology, Beijing 100144, *China*

(Received 9 January 2026; revised manuscript received 7 March 2026; accepted manuscript online 13 March 2026)

The distinct advantage of optogenetic stimulation in precise neuromodulation enables us to dissect the intrinsic mechanisms by which such stimulation of the thalamic reticular nucleus (RE) suppresses epileptic seizures. Since irradiance ($I_{\rm rr}$) is a key factor affecting optogenetic stimulation, we first explore the effect of $I_{\rm rr}$ on epileptic seizures. The results indicate that increasing $I_{\rm rr}$ can suppress the seizures and alter the system's bifurcation structure. The numbers of Hopf bifurcations and saddle–node bifurcations of limit cycles decrease as $I_{\rm rr}$ increases, and the saddle–node bifurcation of the fixed point is a key factor driving the abrupt transition of the system from a high-saturation discharge state to a low-saturation discharge state. Subsequently, we apply optogenetic stimulation in square-wave and Gaussian pulse forms to assess the impacts of three core parameters (pulse width $w_{\rm s}$, pulse frequency f, and $I_{\rm rr}$) on epileptic discharge states. Our numerical simulation results reveal that square-wave pulsed optogenetic stimulation effectively suppresses seizure activity when the pulse width is increased to 15 ms ($f = 40$ Hz, $I_{\rm rr} = 0.3$ mW/mm^2), the pulse frequency to 100 Hz ($w_{\rm s} = 5$ ms, $I_{\rm rr} = 0.3$ mW/mm^2), and the irradiance to 0.8 mW/mm^2 ($w_{\rm s} = 5$ ms, $f = 40$ Hz), respectively. In contrast, using the same analytical method, we find that Gaussian pulsed stimulation requires elevating the respective parameters (pulse width, frequency, irradiance) to 30 ms, 250 Hz, and 1.9 mW/mm^2 for the effective suppression of seizure activity. Therefore, square-wave pulses require a smaller parameter threshold to achieve the effect of inhibiting epileptic seizures. From a physiological perspective, square-wave pulsed optogenetic stimulation is thus more suitable as a potential candidate for clinical trials.

Keywords: optogenetic stimulation, square-wave pulse, Gaussian pulse, bifurcation analysis

PACS: 87.10.Ed, 87.19.lj, 87.19.ll, 87.19.xm

DOI: 10.1088/1674-1056/ae516f **CSTR:** 32038.14.CPB.ae516f

1. Introduction

Epilepsy is a central nervous system disorder characterised by recurrent seizures.[1,2] Currently, commonly used treatments include epilepsy medication, surgery, and neuromodulation.[3] However, many patients develop drug-resistant epilepsy (DRE) and are unresponsive to anti-seizure medications (ASMs). These agents primarily target global neuronal excitability rather than seizure-specific circuit abnormalities.[4] Although surgical resection has its limitations, neuromodulation approaches including DBS and VNS are similarly hindered by a lack of specificity.[5,6] Optogenetics, a relatively novel technology, holds significant potential for neuromodulation therapies, as it can precisely locate the neurons associated with epileptogenic foci while sparing normal brain regions. The principle of optogenetic stimulation (OS) is as follows: a virus is selected as the vector to deliver genes encoding photosensitive proteins into specific target cells, which enables the precise excitation or inhibition of neurons when these cells are exposed to exogenous light of different wavelengths.[7] Channelrhodopsin-2 (ChR2) is a light-gated ion channel protein derived from green algae.[8] As one of the most commonly used genes encoding photosensitive proteins in optogenetic stimulation, it can selectively activate neurons upon blue light illumination, thereby enabling precise spatiotemporal control of neuronal activity.[9] The thalamic reticular nucleus (RE) is a critical hub of the thalamocortical circuit that regulates epilepsy-related synchronization.[10] Optogenetic modulation of the RE can effectively compensate for the limitations of conventional therapies, including pharmacotherapy and surgical intervention, by offering spatiotemporal specificity, cell-type specificity, precise RE targeting, and adjustable stimulation parameters.[11] This approach offers a more targeted and novel strategy for epilepsy treatment.

Optogenetic stimulation features millisecond-scale regulation and high spatiotemporal resolution, which has led to extensive studies on various neurological disorders like epilepsy. In epilepsy-related physiological studies, the efficacy of optogenetic stimulation for epilepsy detection and inhibition has been verified through the targeted stimulation of different brain regions or specific neuronal types. Magnuson *et al.*[12] accomplished the detection and suppression of spontaneous temporal lobe epilepsy via optogenetic stimulation of the hippocampus in mice in 2013. Further, in 2014, they applied optogenetic stimulation to the cerebellum of temporal lobe epilepsy mice and found that cerebellum-targeted inter-

[†]Corresponding author. E-mail: duanlx@ncut.edu.cn

© 2026 Chinese Physical Society and IOP Publishing Ltd. All rights, including for text and data mining, AI training, and similar technologies, are reserved.

vention could inhibit chronic-phase temporal lobe seizures.[13] In 2019, Erofeev *et al.*[14] investigated the relationship between optogenetic stimulation parameters (frequency, duration, and intensity) and neuronal activity by stimulating the hippocampal neurons of mice, identifying the optimal light stimulation parameters for stabilizing neuronal activity. In 2020, Hristova *et al.*[15] found that optogenetic stimulation of medial septal GABAergic neurons could reduce the duration of spontaneous temporal lobe epilepsy through a chronic intrahippocampal kainic acid-induced temporal lobe epilepsy mouse model. In terms of numerical simulation, researchers incorporated the optogenetic modulation mechanism into neuronal dynamic models, thereby providing theoretical support for the optimization of stimulation strategies. Che *et al.*[16] constructed a distributed open-loop optogenetic control strategy by incorporating the ChR2 ion channel model into the Wilson–Cowan model; numerical experiments demonstrated that this control strategy could effectively suppress cortical epileptiform activity in 2017. In 2022, based on the Wilson–Cowan model, Zhang *et al.*[17] performed a comparative analysis of three neuromodulation approaches for epilepsy: optogenetic stimulation (OS), deep brain stimulation (DBS), and electromagnetic induction. They found that OS had distinct superiority over the other two strategies in both stimulation effectiveness and accuracy. Subsequently, in 2023, Zhao *et al.*[18] constructed a corticothalamic model incorporating heterogeneous interneurons to investigate how optogenetic activation of parvalbumin (PV), somatostatin (SOM), and vasoactive intestinal polypeptide (VIP) interneurons modulated the dynamics of absence seizures. The results indicated that PV and SOM interneurons were promising targets for blue-light-mediated seizure control, while the impact of VIP interneurons on seizures was contingent on the inhibitory levels of SOM and PV interneurons. Regarding stimulation modes, square-wave pulses and Gaussian pulses are two widely applied optical pulse forms. Andrasfalvy *et al.*[19] focused on activating ChR2-expressing neurons in mouse hippocampal slices in 2010. By employing Gaussian-pulsed optogenetic stimulation, they realized high-spatiotemporal-resolution targeted activation of ChR2 neurons, thereby achieving precise control over neuronal action potential firing. In 2025, Hyder *et al.*[20] applied square-wave-pulsed optogenetic stimulation to the rats' dorsal striatal neurons; their findings indicated that activating the dorsal striatum could significantly reduce the number and duration of SWDs in absence seizures.

The thalamic reticular nucleus (RE) is an important region located within thalamocortical circuits.[21,22] Most of the RE contains GABAergic neurons, which innervate the thalamus to generate inhibitory postsynaptic potentials (IPSPs) and thereby provide synaptic inhibition to thalamocortical relay neurons.[23] Research findings have demonstrated that enhancing the inhibitory strength of GABAergic neurons within the RE could reduce the duration and intensity of absence seizures.[24] Given that electrically stimulating the RE used in previous studies may induce undesirable side effects, researchers consequently developed optogenetic approaches. In 2011, Halassa *et al.*[25] conducted optogenetic stimulation experiments in freely behaving mice. Their findings demonstrated that transient, selective activation of the RE could convert thalamocortical neuron firing patterns from tonic firing to burst firing and also induce state-dependent neocortical spindle oscillations. In 2013, Paz *et al.*[26] applied optogenetic stimulation to the RE in a rat model of cortical injury and found that reducing thalamic output could rapidly terminate epileptic seizures. Later, in 2017, Chang *et al.*[27] delivered optogenetic stimulation to the RE of transgenic mice, demonstrating that high-frequency, long-duration light stimulation of the RE effectively suppressed cortical epileptiform activity. In 2021, Wicker *et al.*[28] applied optogenetic stimulation in mouse models to investigate the role of the RE in limbic seizures; the results showed that activation of the RE and its midline thalamic projection neurons could inhibit limbic epileptic seizures.

Although optogenetic techniques have been widely applied in the study and treatment of neurological disorders, most studies focus on single stimulation waveforms and lack systematic comparisons and in-depth analysis of dynamic mechanisms. The main innovations of this study are as follows: (1) We construct a modified thalamocortical neural field model integrated with a detailed four-state ChR2 model. (2) We systematically compare the effects of square-wave and Gaussian pulsed stimulations and reveal that square-wave pulses exhibit higher efficiency. (3) We identify the saddle-node bifurcation of limit cycles (LPC) as the key mechanism underlying the state transition from epileptic to normal neural activity. Crucially, these technical and theoretical advances directly tackle three long-standing challenges in epilepsy treatment: insufficient circuit specificity, the dynamic nature of seizures, and limited translation of preclinical research. Our optogenetic modulation of the RE resolves these issues through cell-type-specific and spatiotemporally precise intervention, optimized stimulation parameters integrated with bifurcation analysis, and mechanistic insights derived from preclinical studies that facilitate clinical translation. This work thus provides a targeted approach aimed at meeting the current clinical needs in epilepsy therapy.

Based on the importance of the RE and the temporal and spatial precision of optogenetics, we explore the impacts of optogenetic stimulation targeting the RE on epileptic seizures, as well as the dynamic mechanisms governing seizure state transitions via numerical experiments. The layout of the article is as follows. In Section 2, we provide both the thalamocortical

computational model and the optogenetic stimulation model, along with a detailed specification of all associated parameters. In Section 3, we explore how optogenetic stimulation of the RE affects epileptic seizures and the relevant kinetic mechanisms. Next, we deliver optogenetic stimuli to the RE in the form of square-wave pulses and Gaussian pulses, to evaluate and compare their efficacy in suppressing epileptic seizures. We summarize this article in Section 4.

2. Method and model

2.1. Thalamocortical model

Our study is based on the modified Taylor neural field network model, which consists of a cortical subsystem and a thalamic subsystem, as shown in Fig. 1. The population of excitatory interneurons (EIN), inhibitory interneurons (IN), and excitatory pyramidal (PY) neurons comprises the cortical subsystem, and the thalamic subsystem includes the specific relay nucleus (TC) and RE.

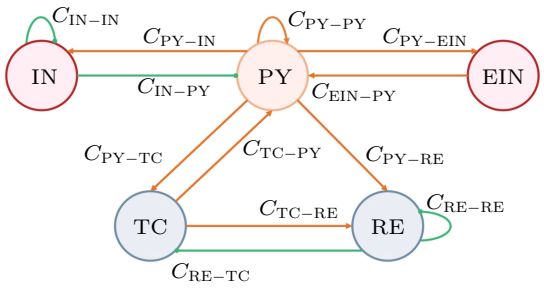


Fig. 1. Diagram of the thalamocortical neural field network model.

Mathematically, it can be described by the following differential equation:

$$\frac{\mathrm{d}PY}{\mathrm{d}t} = \tau_1\big(\varepsilon_1 - PY + C_{\mathrm{PY-PY}}f[PY] - C_{\mathrm{IN-PY}}f[IN] + C_{\mathrm{EIN-PY}}f[EIN] + C_{\mathrm{TC-PY}}f[TC]\big), \quad (1)$$

$$\frac{\mathrm{d}IN}{\mathrm{d}t} = \tau_2\left(\varepsilon_2 - IN + C_{\mathrm{PY-IN}}f[PY] - C_{\mathrm{IN-IN}}f[IN]\right), \quad (2)$$

$$\frac{\mathrm{d}EIN}{\mathrm{d}t} = \tau_3\left(\varepsilon_3 - EIN + C_{\mathrm{PY-EIN}}f[PY]\right), \quad (3)$$

$$\frac{\mathrm{d}TC}{\mathrm{d}t} = \tau_4\left(\varepsilon_4 - TC + C_{\mathrm{PY-TC}}f[PY] - C_{\mathrm{RE-TC}}g[RE]\right), \quad (4)$$

$$\frac{\mathrm{d}RE}{\mathrm{d}t} = \tau_5\big(\varepsilon_5 - RE + C_{\mathrm{PY-RE}}f[PY] + C_{\mathrm{TC-RE}}g[TC] - C_{\mathrm{RE-RE}}g[RE] - U_{\mathrm{ChR2}}\big), \quad (5)$$

where PY, IN, EIN, TC, and RE represent the firing rates of excitatory pyramidal neurons, inhibitory interneurons, excitatory interneurons, specific relay nucleus, and thalamic reticular nucleus, respectively. The terms $-PY$, $-IN$, $-EIN$, $-TC$, and $-RE$ in Eqs. (1)–(5) are linear decay terms that mathematically establish a first-order relaxation dynamics framework, ensuring the existence of stable steady-state solutions for the system. Biologically, they simulate the natural decay of neuronal population activity, provide essential negative feedback, maintain the excitation–inhibition balance of the network, and, together with the time constants, define the dynamic properties of different nuclei.[29–31] $\varepsilon_1, \varepsilon_2, \varepsilon_3, \varepsilon_4, \varepsilon_5$ represent the inputs to different neuron populations, $\tau_1, \tau_2, \tau_3, \tau_4, \tau_5$ are different timescale parameters, $C_{\mathrm{PY-PY}}, \ldots, C_{\mathrm{RE-RE}}$ represent the coupling strength between different neuron populations, $f[\cdot]$ and $g[\cdot]$ is the transfer function, i.e.,

$$f[x] = \frac{1}{1+v^{-x}}, \quad (6)$$

$$g[y] = ay + b, \quad (7)$$

where $x = PY$, IN, EIN, and TC, $y = TC$, RE, $v = 250000$. U_{ChR2} denotes the optogenetic stimulus added to the RE. The values of all constant parameters are shown in Table 1.

Table 1. Parameters in this study.

Parameter	Value	Parameter	Value	Parameter	Value
$C_{\mathrm{PY-PY}}$	1.8	$C_{\mathrm{RE-TC}}$	0.6	ε_2	–3.4
$C_{\mathrm{PY-EIN}}$	0.1	$C_{\mathrm{PY-RE}}$	0–5	ε_3	–0.1
$C_{\mathrm{EIN-PY}}$	0.3	$C_{\mathrm{RE-RE}}$	0.01	ε_4	–2
$C_{\mathrm{PY-IN}}$	4	τ_1	0.026	ε_5	–5
$C_{\mathrm{IN-PY}}$	1.5	τ_2	0.0325	v	250000
$C_{\mathrm{IN-IN}}$	0.05	τ_3	0.026	a	2.8
$C_{\mathrm{PY-TC}}$	3	τ_4	0.0026	b	0.5
$C_{\mathrm{TC-PY}}$	1.2	τ_5	0.0026		
$C_{\mathrm{TC-RE}}$	6–13	ε_1	–0.5		

2.2. Optogenetic model

In past studies, ChR2 has been used as a light-activated channel or transporter protein to regulate neuronal activity.[32–34] Here, referring to the work of Williams *et al.*,[35] we use a four-state model to simulate photocurrent dynamics:

$$\frac{\mathrm{d}O_1}{\mathrm{d}t} = k_1 C_1 - (G_{\mathrm{d1}} + e_{12})O_1 + e_{21}O_2, \quad (8)$$

$$\frac{\mathrm{d}O_2}{\mathrm{d}t} = k_2 C_2 - (G_{\mathrm{d2}} + e_{21})O_2 + e_{12}O_1, \quad (9)$$

$$\frac{\mathrm{d}C_2}{\mathrm{d}t} = G_{\mathrm{d2}}O_2 - (k_2 + G_{\mathrm{r}})C_2, \quad (10)$$

$$\frac{\mathrm{d}p}{\mathrm{d}t} = \left(S_0(\theta) - p\right)/\tau_{\mathrm{ChR2}}, \quad (11)$$

where $O_1 + O_2 + C_1 + C_2 = 1$, O_1, O_2 (C_1, C_2) indicate the fractions of ChR2 channels that are in the open (or closed) state, p is a state variable, k_1, k_2, e_{12}, e_{21}, G_{d1}, G_{d2}, G_{r} denote the jump rates, τ_{ChR2} is the activation time constant of the ChR2 ion channel, $S_0(\theta)$ is the activation function, and its specific expression is $S_0(\theta) = 0.5(1 + \tanh(120(100I_{\mathrm{rr}} - 0.1)))$, which represents an activation ratio between 0 and 1.

Table 2. Optogenetic stimulus-related parameter values.

Parameter	Meaning	Value
k_1	Transition rate of $C_1 \to O_1$	$\varepsilon_1 F p$ (ms^{-1})
k_2	Transition rate of $C_2 \to O_2$	$\varepsilon_2 F p$ (ms^{-1})
ε_1	Quantum efficiency of light absorption in C_1 state	0.8535
ε_2	Quantum efficiency of light absorption in C_2 state	0.14
F	Photon flux	$\sigma_{\rm ret} I_{\rm rr} \lambda/(\omega_{\rm loss} hc)$ (ms^{-1})
$\sigma_{\rm ret}$	Absorption cross section of retinal	10^{-20} m^2
λ	Light wavelength	470 nm
$\omega_{\rm loss}$	Scaling factor of photon loss	1.3
h	Planck's constant	6.626×10^{-34} J·s
c	Light speed	3×10^8 m/s
$G_{\rm d1}$	Transition rate of $O_1 \to C_1$	$0.075 + 0.043\tanh(-(V+20)/20)$ (ms^{-1})
$G_{\rm d2}$	Transition rate of $O_2 \to C_2$	0.05 (ms^{-1})
e_{12}	Transition rate of $O_1 \to O_2$	$0.011 + 0.005\ln(1 + I_{\rm rr}/0.024)$ (ms^{-1})
e_{21}	Transition rate of $O_2 \to O_1$	$0.008 + 0.004\ln(1 + I_{\rm rr}/0.024)$ (ms^{-1})
$\tau_{\rm ChR2}$	Activation time constant of ChR2	1.3 ms
$g_{\rm ChR2}$	Max conductance of ChR2	0.4
γ	Ratio of conductances of O_2/O_1	0.1
$E_{\rm ChR2}$	Reversal potential of ChR2	0 mV
$N_{\rm ChR2}$	Number of ChR2 channels	250
$R_{\rm m}$	Mean resistance of stimulated population	3.2 MΩ
$G_{\rm r}$	Transition rate of $C_2 \to C_1$	$4.34587 \times 10^{-5} \times \exp(-0.0211539274V)$ (ms^{-1})

The form of the ChR2 photocurrent is as follows:

$$I_{\rm ChR2} = g_{\rm ChR2} \cdot G(V) \cdot (O_1 + \gamma O_2) \cdot (V - E_{\rm ChR2}), \quad (12)$$

where V indicates membrane potential, $V = \alpha I - \beta$, I is taken as the firing rate of the RE, $\alpha = 60$ mV, $\beta = 20$ mV. $g_{\rm ChR2}$ denotes the maximum conductance of ChR2. γ is the conductivity ratio of O_2/O_1. $E_{\rm ChR2}$ indicates the reversal potential of ChR2. $G(V)$ is the voltage-dependent rectification function

$$G(V) = \frac{10.6408 - 14.6408 \cdot \exp(-V/42.7671)}{V}. \quad (13)$$

The control potentials induced by photostimulation are as follows:

$$U_{\rm ChR2} = I_{\rm ChR2} \cdot N_{\rm ChR2} \cdot R_{\rm m}/\alpha, \quad (14)$$

where $R_{\rm m}$ is the average resistance of the stimulated population. $N_{\rm ChR2}$ is the number of ChR2 channels per unit area. α normalizes the product of ChR2 photocurrent ($I_{\rm ChR2}$), channel density ($N_{\rm ChR2}$), and average population resistance ($R_{\rm m}$), ensuring $U_{\rm ChR2}$ is dimensionally consistent with other terms in the RE differential equation and mathematically validating our circuit model. The values and specific meanings of the relevant parameters are shown in Table 2.

3. Results

3.1. Optogenetic stimulation of the RE affects the dynamics of seizures

The RE is a vital GABAergic inhibitory nucleus that connects the thalamus and cortex. During epileptic seizures, abnormal activity of the RE may lead to hyperexcitability of neural networks, thereby exacerbating the seizures. Optogenetics combines optical and genetic approaches: it involves constructing gene vectors that express photosensitive proteins in specific neuronal regions and then precisely regulating neuronal activity via exogenous optical irradiation of different wavelengths. Therefore, we apply optogenetic stimulation to the RE and further explore the effects of two RE-associated neuronal pathways, namely, the TC–RE and PY–RE pathways, on epileptic seizures.

3.1.1. The effects of $I_{\rm rr}$ variations on the transition of epileptic seizure states induced by $C_{\rm PY-RE}$

To explore how irradiance $I_{\rm rr}$ modulation affects the discharge transitions of epileptic seizures induced by PY–RE synaptic connection strength ($C_{\rm PY-RE}$), we construct extremum and bifurcation diagrams for $C_{\rm PY-RE}$. Figures 2(a1)–2(a8) show the single-parameter bifurcation analysis of $C_{\rm PY-RE}$ at different $I_{\rm rr}$. Stable and unstable fixed points are denoted by solid red and dashed black lines, respectively, while stable and unstable limit cycles are represented by green and dark blue lines. Regions 1, 3, and 7 are monostable states; regions 2, 4, and 6 are bistable states; and region 5 is a tristable state. Figures 2(b1)–2(b8) show the corresponding extremum diagrams of $C_{\rm PY-RE}$, where the red and blue dots denote local maxima and local minima. The discharge states corresponding to the different regions are as follows: (I) high-saturation discharge state, (II) clonic oscillation, (III) SWD oscillation, (IV, V) 2-SWD oscillation, and (VI) low-saturation discharge state. In addition, we use $(PY + IN)/2$ as the key output metric in our bifurcation analysis, as it effectively characterizes the cortical excitation–inhibition balance and simplifies the dynamical behavior of the high-dimensional system. This setting is

consistently adopted in all subsequent bifurcation analyses.

When $I_{rr} = 0$, the bifurcation diagram and extremum diagram of C_{PY-RE} are shown in Figs. 2(a1) and 2(b1). As C_{PY-RE} increases, the emergence of the saddle-node bifurcation of the limit cycle (LPC1) drives the system into a bistable region composed of a stable limit cycle and a stable fixed point, causing the system's discharge state to transition from high-saturation discharge to clonic oscillation. Subsequently, with a further increase in C_{PY-RE}, the system's discharge state transforms into SWD oscillation under the influence of the Hopf bifurcation (HB1). When C_{PY-RE} continues to rise until HB2 appears, the system's discharge state transitions from SWD oscillation to 2-SWD oscillation. Then, the appearance of LPC2 leads to a transformation into low-amplitude 2-SWD oscillation. Finally, the emergence of LPC4 enables the system to transform into a low-saturation discharge state.

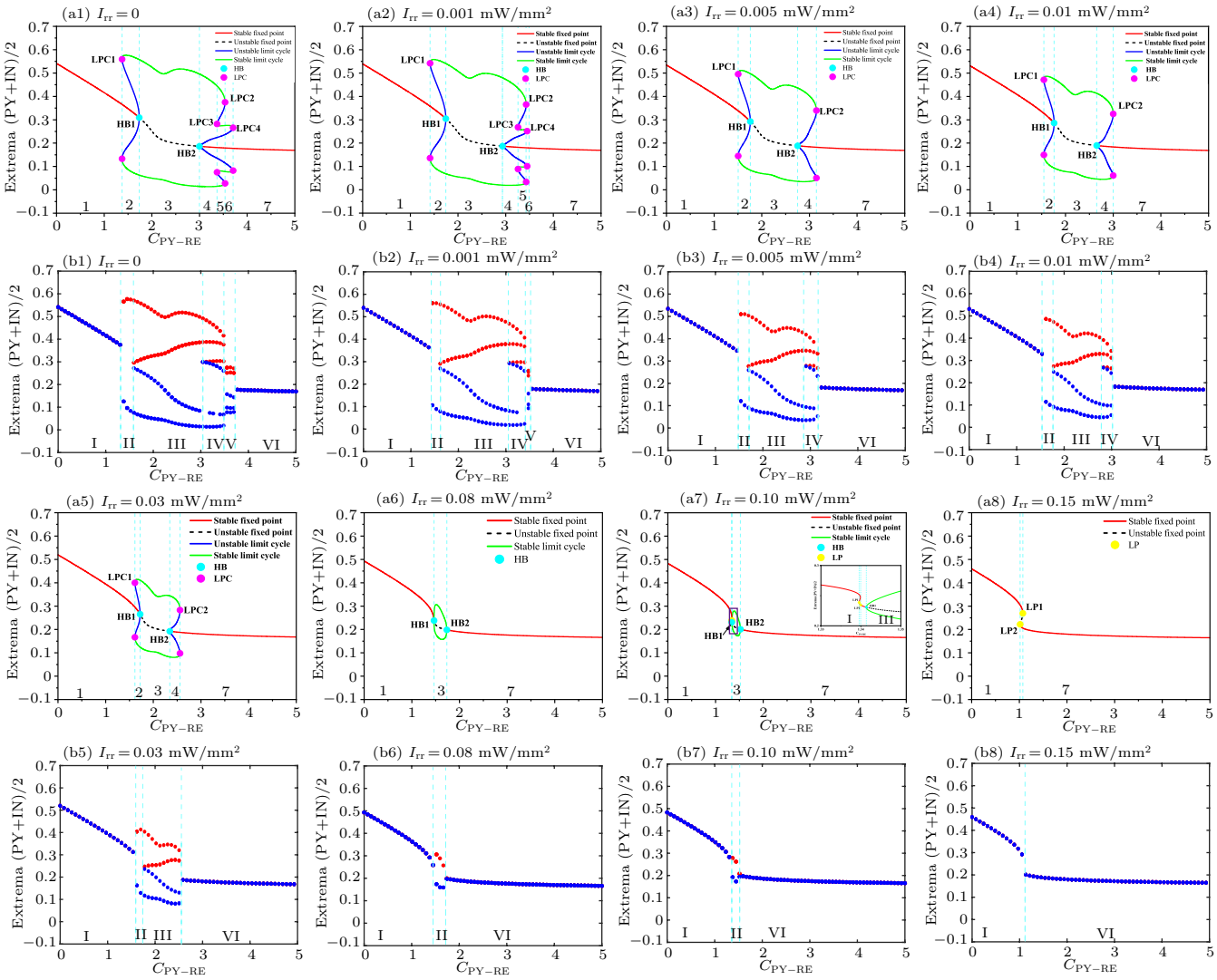


Fig. 2. Single-parameter bifurcation and extremum diagrams for C_{PY-RE}. (a1)–(a8) The single-parameter bifurcation diagrams of C_{PY-RE} for different I_{rr} values. (b1)–(b8) The extremum diagrams of C_{PY-RE} corresponding to the respective I_{rr}. Let $C_{TC-RE} = 9$.

As shown in the bifurcation diagrams of C_{PY-RE} (Figs. 2(a2)–2(a8)), with increasing I_{rr}, the distance between the two HB points diminishes. Meanwhile, the distances between LPC1 and LPC2, as well as between LPC3 and LPC4, also decrease correspondingly. In detail, when the I_{rr} increases to 0.001 mW/mm^2, the left shift of LPC4 reduces the 2-SWD oscillation (Figs. 2(a2) and (b2)). With a further increase in I_{rr} to 0.005 mW/mm^2, LPC3 and LPC4 disappear, leading to the elimination of the low-amplitude 2-SWD oscillation. At this point, the recovery of the system from the 2-SWD oscillation to the low-saturation discharge state is induced by LPC2 (Figs. 2(a3) and 2(b3)). Further increases in I_{rr} progressively reduce the distance between LPC1 and LPC2, causing the system's SWD and 2-SWD oscillations to gradually diminish (Figs. 2(a4)–2(a5) and 2(b4)–2(b5)). As the I_{rr} rises to 0.08 mW/mm^2, LPC1 and LPC2 are eliminated as well. Under this condition, HB1 and HB2 exist within the system, resulting in discharge states comprising saturated discharge and clonic oscillation (Figs. 2(a6) and 2(b6)). With I_{rr} further increasing to 0.1 mW/mm^2, the distance between HB1 and HB2 gradually decreases, contributing to a corresponding reduction in the system's clonic oscillation region. Notably, saddle-node bifur-

cations of the fixed points (LP1 and LP2) emerge in the system at this I_{rr}, yet these bifurcations have no impact on the system's discharge state (Figs. 2(a7) and 2(b7)). As I_{rr} continues to increase, LP1 and LP2 are shifted leftward individually, and the distance between them is found to expand gradually. When the I_{rr} level reaches 0.15 mW/mm^2, HB1 and HB2 disappear completely, such that only LP1 and LP2 remain in the system. The emergence of LP1 and LP2 causes the system to transition directly from a high-saturation discharge state to a low-saturation discharge state (Figs. 2(a8) and 2(b8)). These results indicate that increasing I_{rr} alters the kinetic mechanisms of the system and that appropriate I_{rr} exerts an abolishing effect on seizures induced by C_{PY-RE}.

3.1.2. The effects of I_{rr} variations on the transition of epileptic seizures state jointly induced by C_{PY-RE} and C_{TC-RE}

Optogenetic stimulation of RE enhances the output of its inhibitory neurons, thereby influencing discharge state transitions across the entire brain's neural system through the neural circuits PY–RE and TC–RE (C_{PY-RE} and C_{TC-RE}). Thus, we explore how C_{PY-RE} and C_{TC-RE} jointly modulate the dynamic transition of the system's discharge state after optogenetic stimulation is applied. Figures 3(a1)–3(a8) depict the double-parameter bifurcation diagrams of C_{PY-RE} and C_{TC-RE} under varying I_{rr}. The blue line represents the Hopf bifurcation curve (hb), the black line indicates the saddle-node bifurcation curve of the limit cycle (lpc), and the red line denotes the saddle-node bifurcation curve of the fixed point (lp). Regions MS_1, MS_3, and MS_6 represent monostable regions, regions BS_2 and BS_4 denote bistable regions, and region TS_5 constitutes a tristable region. Figures 3(b1)–3(b8) depict the state diagrams corresponding to different I_{rr}.

Figure 3(a1) depicts the system's dynamical mechanism at $I_{rr} = 0$. Regions MS_1 and MS_6, enclosed by the lpc and the coordinate axes, constitute the monostable regions. At this point, the system's discharge states correspond to high-saturation discharge and low-saturation discharge, respectively. The region MS_3, enclosed by the hb, constitutes a

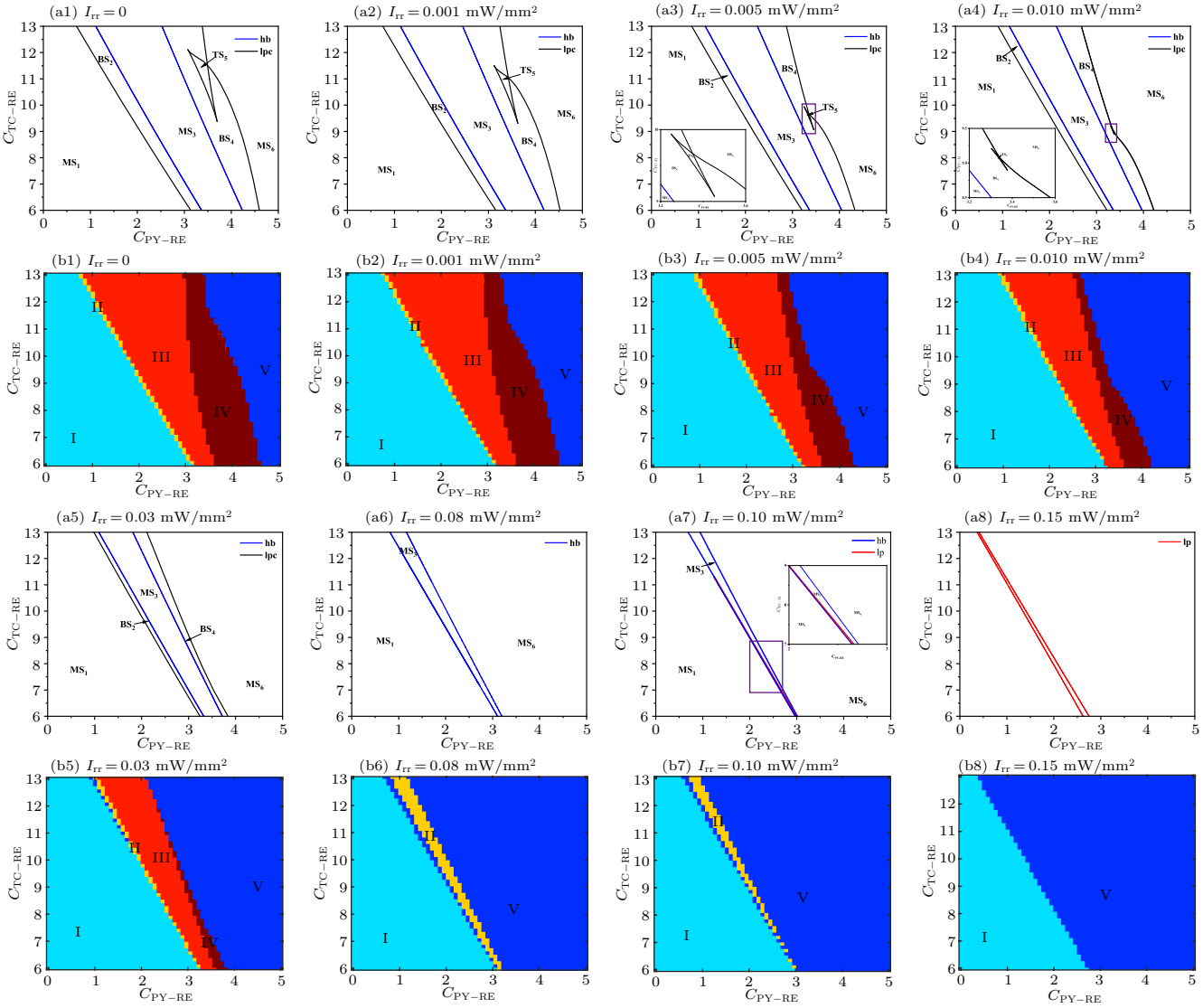


Fig. 3. Bifurcation and state diagrams for C_{PY-RE} and C_{TC-RE}. (a1)–(a8) Bifurcation diagrams for C_{PY-RE} and C_{TC-RE} under different I_{rr}; (b1)–(b8) the corresponding state diagrams.

monostable region. Within this region, only stable limit cycles exist, with the system's discharge state exhibiting SWD and 2-SWD oscillations. Regions BS_2 and BS_4, formed by the lpc and hb, constitute a bistable region. These regions permit the coexistence of stable fixed points and stable limit cycles. The system displays two different discharge states (clonic oscillation and high-saturation discharge) depending on the choice of initial values. A tristable region TS_5 is formed by the lpc. This region comprises two stable limit cycles and a stable fixed point, rendering the system highly susceptible to external stimuli that may induce a transition in its discharge state. Figure 3(b1) shows the state diagram at $I_{rr} = 0$, progressing from left to right as follows: (I) high-saturation discharge, (II) clonic oscillation, (III) SWD oscillation, (IV) 2-SWD oscillation, and (V) low-saturation discharge.

After optogenetic stimulation is applied, as the I_{rr} increases from 0.001 mW/mm^2 to 0.01 mW/mm^2, the sizes of regions BS_4 and TS_5 gradually decrease, thereby leading to a corresponding reduction in the SWD and 2-SWD oscillation regions (Figs. 3(a2)–3(a4) and 3(b2)–3(b4)). When the I_{rr} is further increased to 0.03 mW/mm^2, region TS_5 disappears completely, causing the discharge state in this region to transition back from 2-SWD oscillation to the low-saturation discharge state (Figs. 3(a5) and 3(b5)). As the I_{rr} rises further to 0.08 mW/mm^2, bistable regions BS_2 and BS_4 are eliminated entirely with the disappearance of lpc. The system then retains only monostable regions MS_1, MS_3, and MS_6, with its discharge states showing four modes: high-saturation discharge, clonic oscillation, SWD oscillation, and low-saturation discharge (Figs. 3(a6) and 3(b6)). With the I_{rr} increasing further to 0.1 mW/mm^2, the reduction of the monostable region MS_3 results in a corresponding decrease in the SWD oscillation region. Interestingly, lp emerge in the system at this I_{rr}, while they have no effect on the system's discharge state (Figs. 3(a7) and 3(b7)). When the I_{rr} is increased to 0.15 mW/mm^2, the hb vanishes entirely, eliminating the oscillatory region. The system then exhibits lp, enabling the direct transition from a high-saturation discharge state to a low-saturation discharge state. This effectively controls the system's epileptic state (Figs. 3(a8) and 3(b8)). The results indicate that as I_{rr} increases, the bistable and tristable regions of the system gradually decrease until complete disappearance, which causes corresponding changes in the system's discharge state. Therefore, an appropriate I_{rr} can suppress the seizures jointly induced by C_{PY-RE} and C_{TC-RE}.

3.1.3. Kinetic mechanisms of epileptic seizures affected by optogenetic stimulation

The results above indicate that applying optogenetic stimulation to the RE can suppress the seizures. Moreover, to investigate how optogenetic stimulation affects the kinetic mechanism of epileptic seizures, we conduct single-parameter bifurcation analysis with respect to I_{rr} and double-parameter bifurcation analysis for C_{PY-RE}–I_{rr} and C_{TC-RE}–I_{rr}.

Figure 4 presents the single-parameter bifurcation diagram and extremum diagram for I_{rr}. When I_{rr} is very low, the system resides in a monostable region (1), which is composed of a stable limit cycle, and the discharge state is in the SWD oscillation state. With the increase in I_{rr}, the emergence of the HB gives rise to a bistable region (2) comprising a stable limit cycle and a stable fixed point. At this stage, the system remains in SWD oscillation due to the influence of the stable limit cycle. When the I_{rr} increases to approximately 0.06 mW/mm^2, the emergence of the LPC causes the system to revert to the monostable region (3), which is constituted by a stable fixed point. Under the influence of this stable fixed point, the system recovers to a low-saturation discharge state.

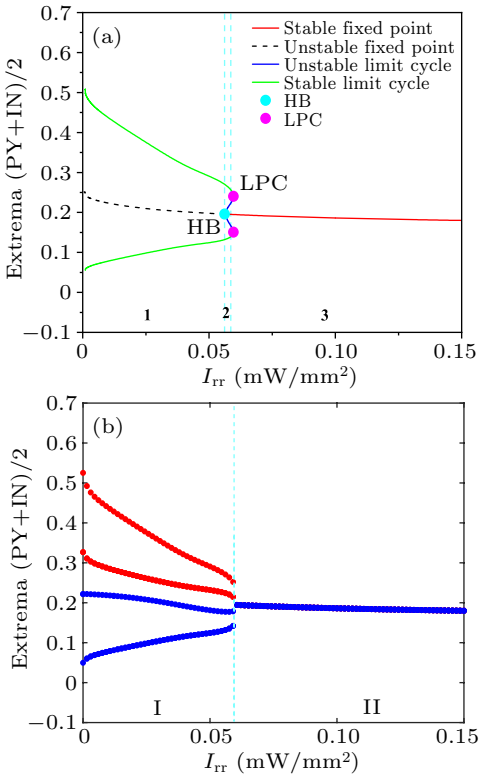


Fig. 4. Single-parameter bifurcation and extremum diagrams for I_{rr}. (a) The red solid line and black dashed line denote stable and unstable fixed points; the blue solid line and green solid line denote unstable and stable limit cycles; the cyan and magenta solid circles denote Hopf bifurcation points and saddle-node bifurcation points of limit cycles, respectively. Regions 1 and 3 constitute monostable regions, while region 2 represents a bistable region. (b) The red and blue solid circles denote the maximum and minimum values of the system output, where region I denotes SWD oscillation, while region II denotes low-saturation discharge state. Let $C_{PY-RE} = 2$, $C_{TC-RE} = 11$.

The joint regulatory effect of C_{PY-RE} and I_{rr} is illustrated in Fig. 5(b). The plane is divided into multiple colored regions: regions I and V represent high-saturation and low-saturation discharge states, where no epileptic seizures occur; regions II, III, and IV denote clonic oscillation, SWD oscillation, and 2-SWD oscillation, respectively. Figure 5(a) shows the double-

parameter bifurcation analysis under the combined influence of $C_{\mathrm{PY-RE}}$ and I_{rr}. The plane is partitioned into multiple regions, including bistable regions where stable limit cycles and stable fixed points coexist, as well as monostable regions where only stable limit cycles or stable fixed points exist. The red line denotes lp, marking the critical threshold for sudden changes in fixed point stability. The blue line represents hb, signifying the emergence or disappearance of limit cycles. The black line indicates lpc, meaning the critical threshold for sudden changes in limit cycle stability. These lines visually depict the various bifurcation events associated with the existence and stability of limit cycles and fixed points within the system. When I_{rr} is low, the system undergoes two types of bifurcations, namely, lpc and hb. The discharge state exhibits high-saturation discharge, clonic oscillation, SWD oscillation, 2-SWD oscillation, and low-saturation discharge, indicating that transitions between saturation discharge and epileptic states are caused by the emergence and disappearance of lpc. As I_{rr} increases, lpc and hb gradually disappear, giving way to lp. The system resides in the regions of high-saturation and low-saturation discharge states, which signifies that the transition between these two states is induced by lp. The above-mentioned results indicate that the discharge state of the system is related to these bifurcation curves.

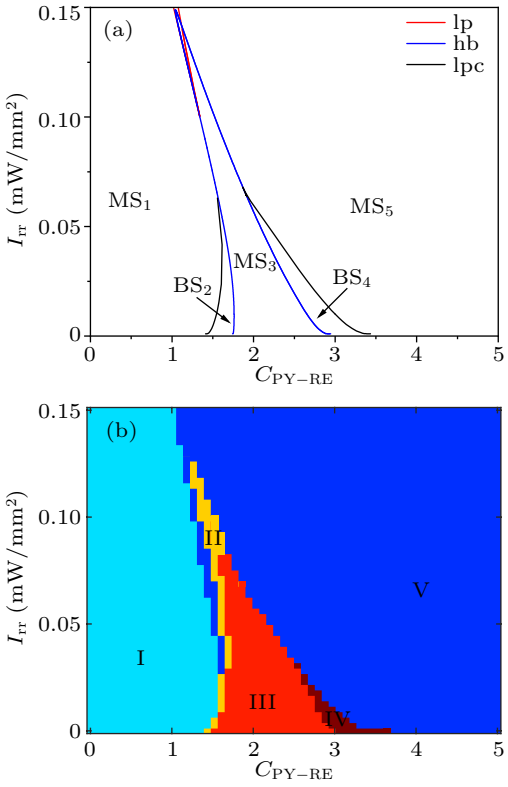


Fig. 5. Bifurcation and state diagrams of $C_{\mathrm{PY-RE}}$ and I_{rr}. (a) MS_1, MS_3, and MS_5 are monostable regions, BS_2 and BS_4 are bistable regions; red, blue, and black lines represent saddle-node bifurcation curves of the fixed points (lp), Hopf bifurcation curves (hb), and saddle-node bifurcation curves of limit cycles (lpc), respectively. (b) The different colored regions in the figure represent high-saturation discharge state (I), clonic oscillation (II), SWD oscillation (III), 2-SWD oscillation (IV), and low-saturation discharge state (V). Let $C_{\mathrm{PY-RE}} = 2$.

The double-parameter bifurcation analysis of $C_{\mathrm{TC-RE}}$ and I_{rr} is shown in Fig. 6(a), with the corresponding discharge states depicted in Fig. 6(b). Regions MS_1 and MS_5 are monostable regions formed by stable fixed points, corresponding to high-saturation and low-saturation discharge states (I and IV). The regions BS_2 and BS_4, formed by lpc and hb, constitute a bistable region where stable fixed points and stable limit cycles coexist. At this point, due to the influence of hb, the system exhibits clonic oscillation (II). The region MS_3, formed solely by hb, constitutes a monostable region comprised exclusively of stable limit cycles. In this region, the system exhibits the SWD oscillation (III) state due to the influence of the stable limit cycles. When I_{rr} is high, the emergence of the lp enables the system to transition directly from a high-saturation discharge state to a low-saturation discharge state. These results reveal that the magnitude of the I_{rr} and the value of $C_{\mathrm{TC-RE}}$ influence the discharge state and bifurcation phenomena of the system.

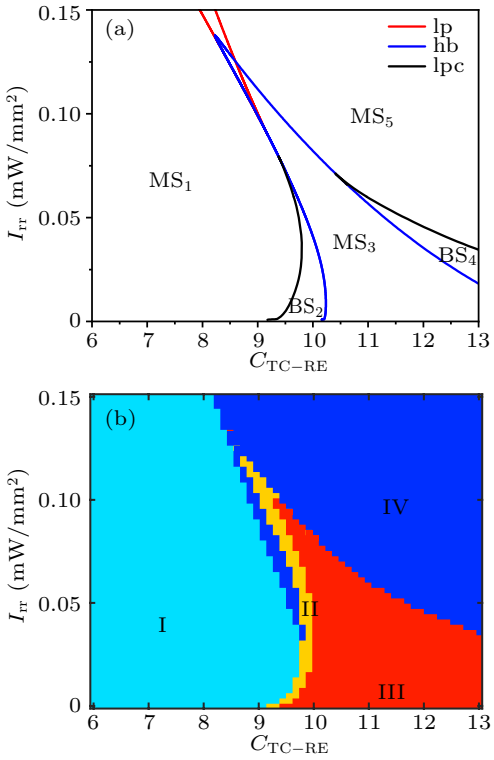


Fig. 6. Bifurcation and state diagram of $C_{\mathrm{TC-RE}}$ and I_{rr}. (a) MS_1, MS_3, and MS_5 are monostable regions, while BS_2 and BS_4 are bistable regions; red, blue, and black lines represent saddle-node bifurcation curves of the fixed points (lp), Hopf bifurcation curves (hb), and saddle-node bifurcation curves of limit cycles (lpc), respectively. (b) The different colored regions in the figure represent high-saturation discharge state (I), clonic oscillation (II), SWD oscillation (III), and low-saturation discharge state (IV). Let $C_{\mathrm{PY-RE}} = 2$.

The above results indicate that activation of RE neurons via optogenetic techniques enhances their inhibitory output, thereby reducing the abnormal information transmission between the thalamus and the cortex. This simultaneously reveals that LPC, HB, and LP are key factors affecting the transition of epileptic discharge states. Thus, an appropriate I_{rr} can be selected and can effectively suppress the seizures.

3.2. The effects of square-wave pulsed optogenetic stimulation on epileptic seizures

Brain neuronal activity is inherently rhythmic, and the application of pulsed optical stimulation can achieve synchronization with these natural rhythms, thereby enhancing the regulatory effect while reducing the interference of optical stimulation with normal neural functions. Research by Himanshu Bansal *et al.*[36] demonstrated that optical pulses of different shapes exert distinct effects on neurons expressing ChR2. Based on the core conclusion of the study that an optical pulse waveform is a determinant of photosensitive neuronal responses, we surmise that square-wave and Gaussian pulsed stimulations might differentially affect epileptic seizure activity. We thus separately examine the effects of square-wave and Gaussian pulsed optogenetic stimulation on epileptic seizure activity.

The initial stimulation parameters, $w_s = 5$ ms, $f = 40$ Hz, and $I_{rr} = 0.3$ mW/mm^2, are chosen based on previous experimental studies. A pulse width of 5 ms was selected based on the study by Gradinaru *et al.*, who reported that 2–10 ms represents the optimal range for ChR2-mediated activation of the RE, and that 5 ms is sufficient to achieve full activation of ChR2.[37–40] A pulse frequency of 40 Hz was adopted based on the work of Pinault *et al.*, as this frequency matches the natural firing frequency of the RE (35–45 Hz). This choice avoids unwanted desynchronization of the thalamocortical circuit and effectively suppresses abnormal neural synchronization linked to epileptiform activity.[41–44] An irradiance of 0.3 mW/mm^2 was adopted following Gradinaru *et al.*, who demonstrated that pulsed stimulation required a relatively high peak irradiance to evoke neural activation comparable to that induced by continuous stimulation.[45] Together, these parameter selections ensure the physiological validity and experimental rationality of our numerical simulations.

3.2.1. Square-wave pulsed photocurrents

Square-wave pulses are the most commonly employed pulse waveform in optogenetic stimulation. They maintain a constant I_{rr} throughout the duration of the optical pulse, enabling rapid activation and inhibition of neuronal activity. The mathematical expression takes the following form:

$$I_{light}(t) = \begin{cases} 1, & t_1 < t < t_2, \\ 0, & \text{otherwise}, \end{cases} \tag{15}$$

where $I_{light}(t)$ denotes the variation of photocurrent over time, $w_s = t_2 - t_1$ indicates the pulse width, and t_1 and t_2 denote the duration of the optical pulse on and off, respectively.

Since optical pulse signals undergo temporal variations influenced by pulse width (w_s), pulse frequency (f), and I_{rr}, thereby generating distinct forms of photocurrent that subsequently affect the discharge state of epileptic seizures, we investigate the impact of altering these three optical pulse signal parameters on the epileptic discharge state. To visually depict the system's discharge state following optogenetic stimulation and express the ChR2 photocurrent, we select an initial state of SWD oscillation and apply optogenetic stimulation at $t = 10000$ ms. The results are shown in Fig. 7(a). Following application of square-wave pulsed optogenetic stimulation, the system gradually recovers from SWD oscillation to a low-saturation discharge state. Figure 7(b) shows a localized enlargement of the interval $[29500, 30000]$, from which we can observe the form of the photocurrent expressed by ChR2. Subsequently, we explore in detail the effects of altering the parameters of optical pulse signals on the state of epileptic discharges arising from the combined action of C_{PY-RE} and C_{TC-RE}.

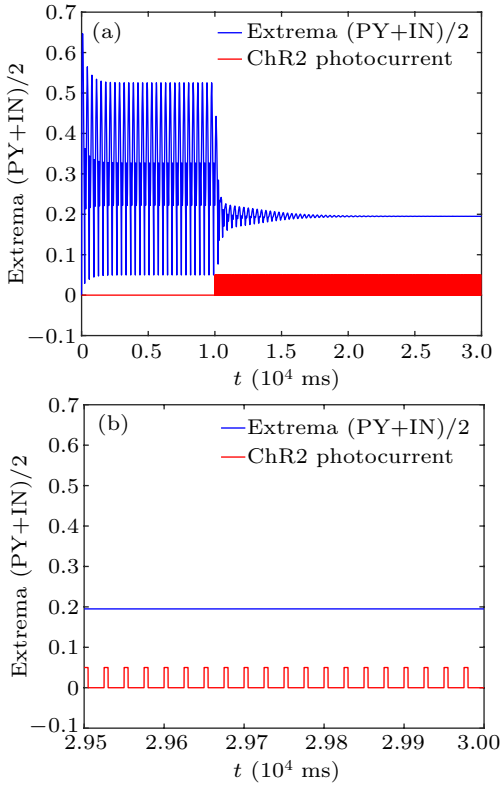


Fig. 7. Time-series diagram following the application of square-wave pulsed optogenetic stimulation. The blue line represents the system's output signal value, while the red line denotes the output signal value for the ChR2 photocurrents. Let $C_{PY-RE} = 2$, $C_{TC-RE} = 11$, $w_s = 5$ ms, $f = 40$ Hz, $I_{rr} = 0.3$ mW/mm^2.

3.2.2. The effect of modifying optical pulse signal parameters on epileptic discharge states

We study the effect of I_{rr} solely on the epileptiform discharge state and its kinetic mechanisms induced jointly by C_{PY-RE} and C_{TC-RE} in Subsection 3.1. In this section, we continue to investigate the effects of variations in w_s, f, and I_{rr} on epileptic seizures, as well as the optimal parameter values capable of suppressing the seizures.

Figure 8 investigates the effects of altering w_s on epileptic discharge states induced by C_{PY-RE} and C_{TC-RE}, while maintaining a fixed f and I_{rr}. Figure 8(a) depicts the system's

discharge states under optical pulse parameters of $w_s = 5$ ms, $f = 40$ Hz, and $I_{rr} = 0.3$ mW/mm^2. From left to right, the four discharge states are: high-saturation discharge, clonic oscillation, SWD oscillation, and low-saturation discharge. With the increase in w_s, the discharge state also undergoes corresponding changes. At $w_s = 8$ ms, the SWD oscillation region diminishes significantly (Fig. 8(b)). Continuously increasing to $w_s = 10$ ms causes the SWD oscillation region to vanish and the clonic oscillation region to diminish (Fig. 8(c)). Until $w_s = 15$ ms, the clonic oscillation region ceases, and the system's discharge state manifests as high-saturation and low-saturation discharges, with the epileptic state being completely suppressed. It can be seen that as w_s increases, the system is enabled to recover from the epileptic state to a saturated discharge state.

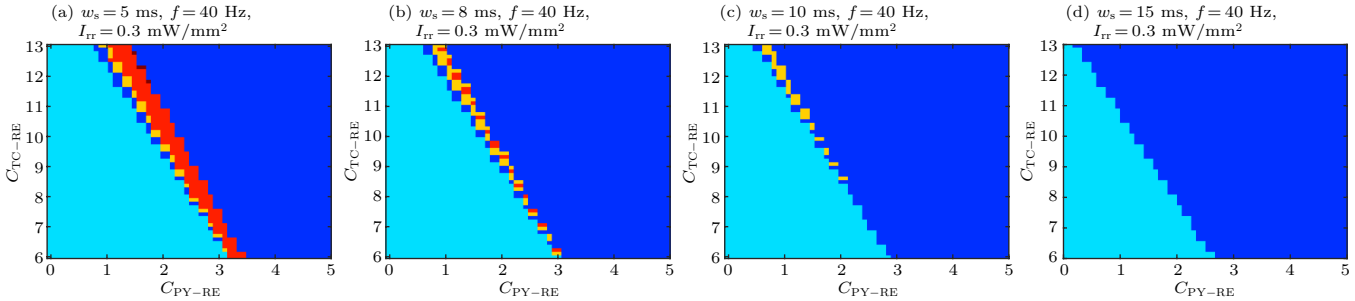


Fig. 8. Pulse width (w_s) variation affects the discharge state diagrams of epileptic seizures.

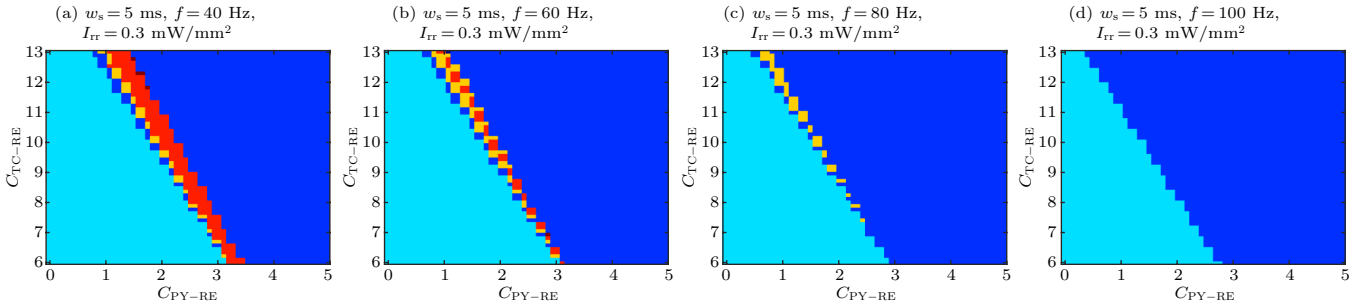


Fig. 9. Pulse frequency (f) variation affects the discharge state diagrams of epileptic seizures.

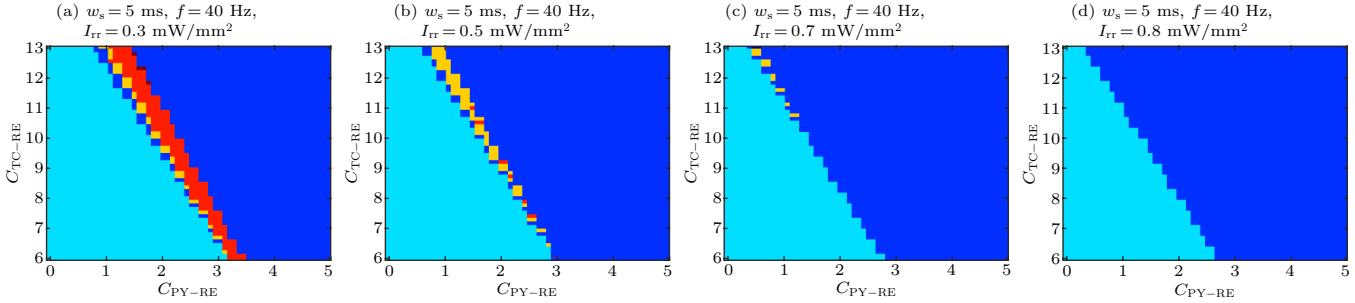


Fig. 10. The I_{rr} variation affects the discharge state diagrams of epileptic seizures.

Figure 9 illustrates the state diagrams of epileptic seizures when w_s and I_{rr} remain constant, where only f is altered. In Fig. 9(a), the optical pulse signal parameters are as follows: $w_s = 5$ ms, $f = 40$ Hz, $I_{rr} = 0.3$ mW/mm^2. Figures 9(b)–9(d) show the system's discharge state after increasing f. With the increase of f, at $f = 60$ Hz, the SWD oscillation region is significantly reduced; at $f = 80$ Hz, the SWD oscillation region disappears entirely. Further increasing f to 100 Hz causes the system's clonic oscillation state to disappear entirely, leaving only the saturated discharge state. This demonstrates that increasing f alone can suppress the seizures.

We explore the effect of altering only the I_{rr} on epileptic seizures. In Fig. 10(a), the optical pulse signal parameters are $w_s = 5$ ms, $f = 40$ Hz, $I_{rr} = 0.3$ mW/mm^2. Figures 10(b)–10(d) show the discharge states of C_{PY-RE} and C_{TC-RE} after altering the I_{rr}. As I_{rr} increases, the regions exhibiting SWD oscillation and clonic oscillation gradually diminish. Upon reaching $I_{rr} = 0.8$ mW/mm^2, the system's discharge state manifests as two distinct discharge states: low-saturation discharge and high-saturation discharge. Similar to the preceding two situations, it follows that increasing I_{rr} can also suppress epileptic seizures.

3.2.3. The effect of correlation relationships in optical pulse signal parameters on epileptic seizures

The findings above show that increasing either w_s, f, or I_{rr} alone can suppress epileptic seizures. Subsequently, we investigate the correlations between these three factors influencing epileptic seizures by using square-wave pulsed optogenetic stimulation at $C_{TC-RE} = 11$ and $C_{PY-RE} = 2$.

Figure 11(a) demonstrates how the correlation between f and I_{rr} affects epileptic seizures for a fixed $w_s = 5$ ms. When $f < 20$ Hz, whatever the increase in I_{rr}, the system exhibits SWD oscillation without entering a low-saturation discharge state. It can be concluded that the system's epileptic state remains unsuppressed if f is too low. Similarly, when $I_{rr} < 0.1$ mW/mm^2, the system will not exhibit the low-saturation discharge state regardless of how high f is increased. This also means that even an excessively low I_{rr} cannot restore the system from the epileptic state to a low-saturation discharge state. When $f > 20$ Hz and $I_{rr} > 0.1$ mW/mm^2, the system enters the low-saturation discharge state. This indicates that for a fixed $w_s = 5$ ms, the suppression of epileptic states exhibits a positive correlation between f and I_{rr}.

Figure 11(b) shows the relationship between w_s and I_{rr} at a fixed $f = 40$ Hz. When w_s is too small or I_{rr} is too low, the system exhibits SWD oscillation. At this point, increasing the value of the other parameters will not generate a low-saturation discharge state. The system exhibits a low-saturation discharge state when $w_s > 2$ ms or $I_{rr} > 0.1$ mW/mm^2, thereby suppressing the system's epileptic state.

Figure 11(c) investigates the relationship between w_s and f at $I_{rr} = 0.3$ mW/mm^2. When f is very low, the system may exhibit SWD oscillation instead of the low-saturation discharge state. When w_s is very low, no matter how much f is increased, the system's discharge state manifests as SWD oscillation rather than low-saturation discharge. The low-saturation discharge state occurs when $f > 20$ Hz and $w_s > 2$ ms. This indicates that the suppression of epileptic states within the system is contingent upon the selection of optical pulse signal parameters, with one parameter remaining constant while the other two exhibit an approximate positive correlation.

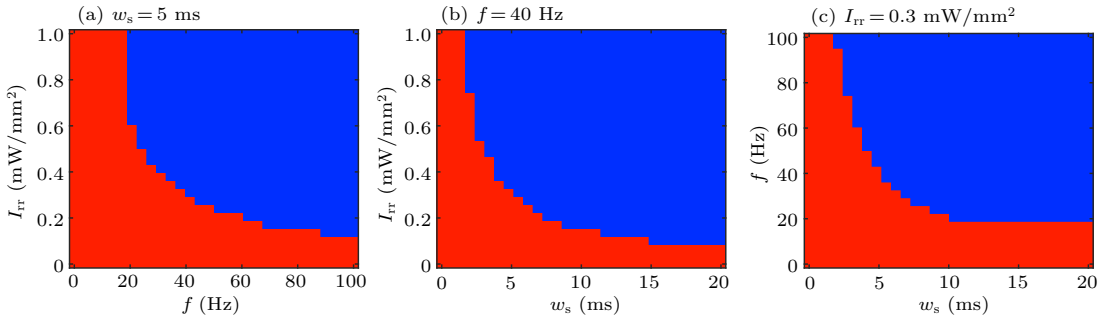


Fig. 11. Discharge state diagrams about w_s, f, and I_{rr} affecting epileptic seizures.

These results specify the parameter range that enables square-wave pulsed optogenetic stimulation of RE to suppress epileptic seizures efficiently. Excessively low values of w_s, f, and I_{rr} would render the stimulation ineffective in inhibiting epileptic seizures.

3.3. The effects of Gaussian pulsed optogenetic stimulation on epileptic seizures

3.3.1. Gaussian pulsed photocurrents

Gaussian pulses are another commonly employed pulse form, whose optical current exhibits temporal variation following a Gaussian distribution curve. They possess favorable directionality and demonstrate good tissue penetration within a certain range. Their mathematical expression is

$$I_{light}(t) = \begin{cases} \exp\left(-\dfrac{(t-t_0)^2}{2\delta^2}\right), & t_1 < t < t_2, \\ 0, & \text{otherwise}, \end{cases} \tag{16}$$

where $I_{light}(t)$ represents the variation of the photocurrent over time, t_0 denotes the center of the Gaussian distribution, and δ is the standard deviation (used here to control the pulse width, $\delta = w_s/7$, $w_s = t_2 - t_1$), while t_1 and t_2 mean the duration of the light pulse on and off, respectively.

The photocurrent behavior of Gaussian pulses depends closely on the selection of w_s, f, and I_{rr}. Similar to square-wave pulsed optogenetic stimulation, we plot a time-series diagram of the initial state undergoing SWD oscillation with optogenetic stimulation applied at $t = 10000$ ms, as shown in Fig. 12(a). Figure 12(b) shows a local magnification in the interval [29500, 30000]. The system's discharge state after applying optogenetic stimulation in the form of Gaussian pulses remains SWD oscillation: only the amplitude range of the oscillation is reduced, but the epileptic state is not suppressed.

3.3.2. Variations in optical pulse signal parameters influencing epileptic seizures and their interrelationships

Compared to square-wave pulsed optogenetic stimulation, Gaussian pulsed optogenetic stimulation more readily mimics transient stimulation. We similarly explore the ef-

fects of three influencing factors (w_s, f, and I_{rr}) on epileptic seizures, along with the correlations among these variables.

We first explore the impact of varying w_s on an epileptic discharge state for a certain f and I_{rr}. Figure 13(a) depicts the discharge states of C_{PY-RE} and C_{TC-RE} for optical pulse parameters of $w_s = 5$ ms, $f = 40$ Hz, $I_{rr} = 0.3$ mW/mm^2. From left to right, the discharge sequentially transitions through five distinct states: high-saturation discharge, clonic oscillation, SWD oscillation, 2-SWD oscillation, and low-saturation discharge. When w_s is increased to 15 ms, the 2-SWD oscillation region is significantly reduced; while the system's epileptic activity persists throughout, a further increase to 30 ms results in the system exhibiting a fully saturated discharge state. Compared to square-wave pulsed optogenetic stimulation, Gaussian pulsed optogenetic stimulation requires a greater w_s for complete recovery to the normal state.

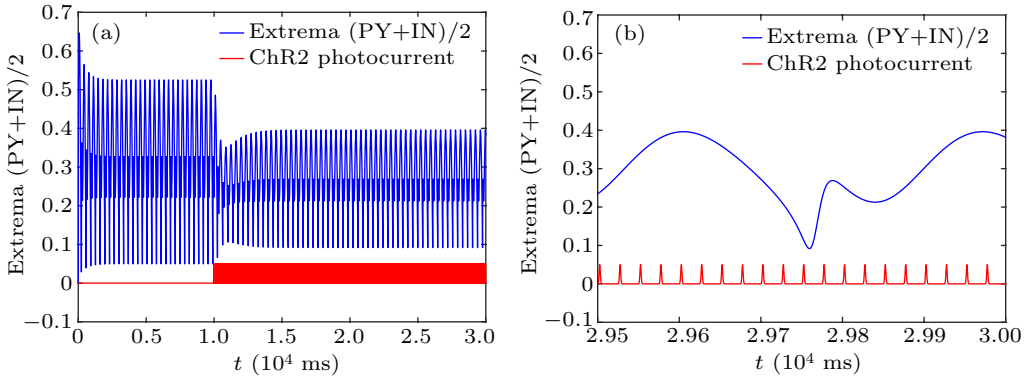


Fig. 12. Time-series diagram following the application of Gaussian pulsed optogenetic stimulation. The blue line represents the system's output signal value, while the red line denotes the output signal value for the ChR2 photocurrents. Let $C_{PY-RE} = 2$, $C_{TC-RE} = 11$, $w_s = 5$ ms, $f = 40$ Hz, $I_{rr} = 0.3$ mW/mm^2.

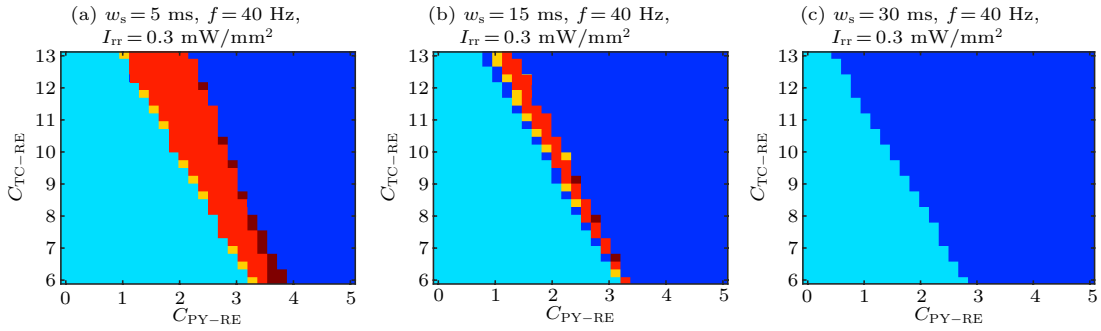


Fig. 13. Pulse width (w_s) variation affects the discharge state diagrams of epileptic seizures.

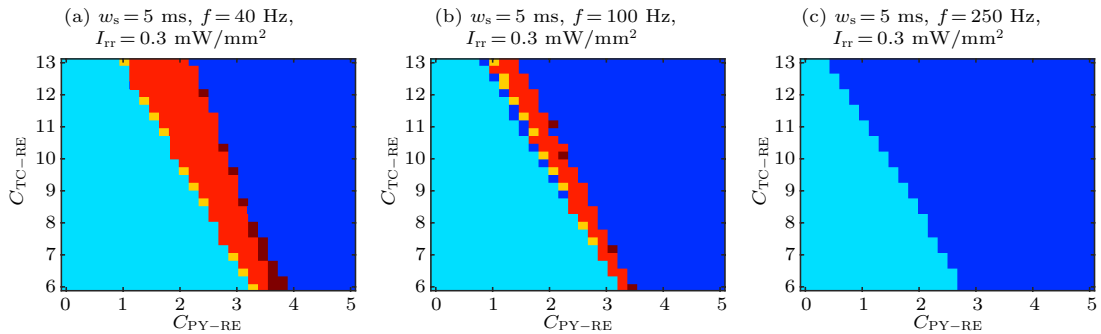


Fig. 14. Pulse frequency (f) variation affects the discharge state diagrams of epileptic seizures.

Secondly, we study the influence of changing only f on an epileptic discharge state. Figure 14(a) shows the system's discharge state under optical stimulation parameters of $w_s = 5$ ms, $f = 40$ Hz, $I_{rr} = 0.3$ mW/mm^2. Figures 14(b) and 14(c) show the state diagrams after increasing f. As f increases to 100 Hz, the SWD oscillation and 2-SWD oscillation regions increase prominently, but it fails to suppress the seizures. By this time, optogenetic stimulation with square-wave pulses can restore the system to a normal state. Upon further increasing to $f = 250$ Hz, the system fully recovers to a saturated discharge state. However, f becomes excessively high and poses a risk to the body, rendering it unsuitable for clinical application.

Thirdly, we research the effect of only varying I_{rr} on suppressing seizures. Figure 15(a) shows the state diagram for optical pulse signal parameters of $w_s = 5$ ms, $f = 40$ Hz, and $I_{rr} = 0.3$ mW/mm^2. Upon increasing I_{rr} to 0.8 mW/mm^2, there is a significant reduction in the epileptic state region, but it does not disappear. When the I_{rr} is further increased to 1.9 mW/mm^2, the system's epileptic state is completely suppressed. In this case, however, I_{rr} is excessively high, such that the instantaneous high-intensity stimulation causes unintended physiological consequences, so it cannot be directly implemented in physiological assays.

Finally, we separately investigate the influence of any two of the following parameters on the system's discharge state: w_s, f, and I_{rr}. At $w_s = 5$ ms, the effect of f and I_{rr} on the system's discharge state is shown in Fig. 16(a). When f or I_{rr} is too low, the system exhibits SWD oscillation without entering the low-saturation discharge state. When both I_{rr} and f are high, the system enters the low-saturation discharge state. Figure 16(b) demonstrates how w_s and I_{rr} correlate with epileptic seizures for a fixed $f = 40$ Hz. As I_{rr} and w_s both increase substantially, the system exhibits the low-saturation discharge state. At $I_{rr} = 0.3$ mW/mm^2, the discharge state diagram concerning epileptic seizures between w_s and f is given in Fig. 16(c). Unlike optogenetic stimulation in the form of square-wave pulses, as the system state transitions from the bottom-left to the top-right of the panel, its discharge mode experiences a sequential dynamic transition from SWD oscillation to low-saturation discharge and then back to SWD oscillation. This phenomenon indicates that excessively high or low values of either f or w_s can induce the occurrence of SWD oscillation. In addition, these findings further reveal that precise selection of optical pulse parameters is essential to effectively suppress epileptic seizures. Any parameter among w_s, f, and I_{rr} that falls outside the appropriate range renders the suppression of epileptic seizures unachievable.

The findings demonstrate that Gaussian pulsed optogenetic stimulation demands higher parameter settings than square-wave pulsed optogenetic stimulation to exert effective control of epileptic seizures. Meanwhile, this study further reveals that optogenetic stimulation with different waveforms exhibits significant differences in its efficacy for regulating epileptic seizures, and the selection of specific protocols should be comprehensively considered in combination with experimental situations and application requirements.

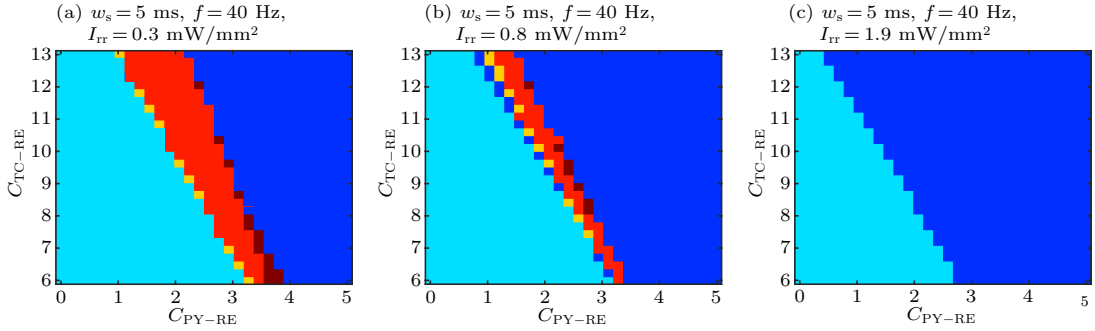


Fig. 15. The I_{rr} variation affects the discharge state diagram of epileptic seizures.

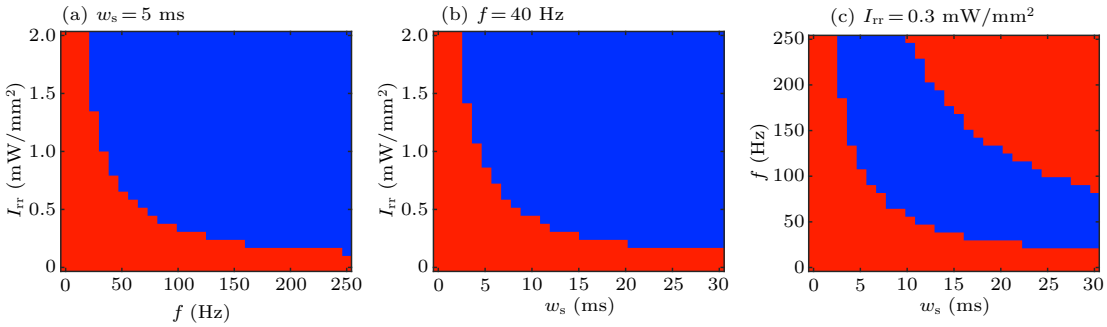


Fig. 16. Discharge state diagrams about w_s, f, and I_{rr} affecting epileptic seizures.

4. Conclusion

Using a thalamocortical neural field network model, we employ optogenetic stimulation of the RE to investigate the dynamic mechanisms governing seizure modulation induced by the excitatory pathways PY–RE and TC–RE.

Firstly, we apply sustained optogenetic stimulation to the RE to elucidate the intrinsic dynamic mechanisms that govern how this stimulation regulates epileptiform discharge states. Without optogenetic stimulation, the system's discharge state is affected by four LPCs and two HBs in the pathway PY–RE. With the application of optogenetic stimulation (i.e., an increase in I_{rr}), the number of bifurcation points gradually

decreases. When I_{rr} reaches 0.15 mW/mm^2, HB and LPC completely disappear. At this time, the emergence of an LP leads the discharge state to transition directly from a high-saturation discharge to a low-saturation discharge state. We further explore the action mechanisms of optogenetic stimulation on epileptic seizures induced by two excitatory pathways C_{PY-RE} and C_{TC-RE}. Through double-parameter bifurcation diagrams we find that the bistable and tristable regions constitute the primary regions for epileptic seizures. An increase in I_{rr} causes the tristable and bistable regions to disappear successively, thereby altering the system's discharge state. This transition shifts the discharge state from high-saturation discharge, clonic oscillation, SWD oscillation, 2-SWD oscillation, and low-saturation discharge to the state characterised by high-saturation and low-saturation discharges.

Second, we explore the bifurcation analysis of I_{rr} for epileptic seizures, where it is shown that the LPC is the critical factor underlying the system's transition from the epileptic state to the normal state through single-parameter bifurcation analysis of I_{rr}. Further double-parameter bifurcation analyses of C_{PY-RE}–I_{rr} and C_{TC-RE}–I_{rr} reveal that hb mediates the switching of the system's discharge state from clonic oscillation to SWD oscillation. These analyses concomitantly demonstrate that as I_{rr} increases, the system undergoes bidirectional state transitions between the physiological normal state and the pathological epileptic state. When I_{rr} reaches a specific threshold, the system stabilizes in the physiological normal state (Figs. 5(a) and 6(a)).

Finally, on the basis of the rhythmic nature of biological neural activity, we apply optogenetic stimulation in the form of pulses to the RE and explore its effects on an epileptic discharge state. Herein, we systematically evaluate the modulatory effects of square-wave pulsed optogenetic stimulation on epileptiform seizure activity in the thalamocortical neural circuit model. We find that when $f = 40$ Hz and $I_{rr} = 0.3$ mW/mm^2 are fixed, increasing w_s from 5 ms to 15 ms changes the system's firing modes from four states (high-saturation discharge, clonic oscillation, SWD oscillation, and low-saturation discharge) to two states (high-saturation discharge and low-saturation discharge), thereby achieving the effect of suppressing the seizures. Similarly, when $w_s = 5$ ms and $I_{rr} = 0.3$ mW/mm^2 are fixed, increasing f from 40 Hz to 100 Hz also restores the system's discharge state to the normal background state. In addition, when $w_s = 5$ ms and $f = 40$ Hz are fixed, increasing I_{rr} from 0.3 mW/mm^2 to 0.8 mW/mm^2 can also realize the control of epileptic seizures. These results demonstrate that increasing the value of one parameter can effectively suppress the seizures when the other two parameters are kept constant. Furthermore, we analyze the relationship between w_s, f, and I_{rr}. When one parameter is fixed, epileptic seizures are induced if the other two parameters are small, and controlled if the other two parameters are large. As it is another commonly used pulse form, we also explore the effects of Gaussian pulses on epileptic discharge states. Similar to square-wave pulsed optogenetic stimulation, increasing w_s, f, or I_{rr} individually can suppress the seizures. However, square-wave pulsed optogenetic stimulation exhibits a lower parameter threshold for seizure inhibition, rendering it more suitable as a clinical option.

In conclusion, our study further clarifies the mechanisms underlying optogenetic regulation of epileptic seizures: LPC acts as the critical bifurcation node that gates the transition from the epileptic to the physiological state, while HB mediates the switching between clonic and SWD oscillations within the pathological regime. As I_{rr} increases, the gradual elimination of bistable and tristable regions in the circuit directly disrupts the dynamical basis for seizure genesis, thereby establishing a mechanistic relationship between stimulation intensity and circuit stability. From a clinical translation perspective, square-wave pulses exhibit distinct advantages: they feature a lower seizure inhibition threshold and achieve robust seizure control with reduced energy delivery and minimized off-target effects, thus providing critical guidance for the design of implantable optogenetic devices. Despite the promising results, several challenges remain for clinical translation, including the precision of gene delivery, potential phototoxicity, long-term stability, and safety validation in large animals. Future studies will focus on these issues.

Acknowledgement

This work is supported by the National Natural Science Foundation of China (Grant No. 12272002).

References

[1] Fisher R S, van Emde Boas W, Blume W, Elger C, Genton P, Lee P and Engel J 2005 *Epilepsia* **46** 470
[2] Yuan Z, Du M, Yu Y and Wu Y 2023 *Chin. Phys. B* **32** 020502
[3] Yan L, Zhang H and Sun Z 2024 *Chin. Phys. B* **33** 058703
[4] Ghosh S, Sinha J K, Ghosh S, Sharma H, Bhaskar R and Narayanan K B 2023 *Brain Sci.* **13** 1305
[5] Engel J J, Wiebe S, French J, Sperling M, Williamson P, Spencer D, Gumnit R, Zahn C, Westbrook E and Enos B 2003 *Neurology* **60** 538
[6] Lüscher C, Emiliani V, Farahany N, Gittis A, Gradinaru V, High K A, Roska B, Sahel J A, Yizhar O and Zeng H 2025 *Nat. Neurosci.* **28** 2415
[7] Yizhar O, Fenno L E, Davidson T J, Mogri M and Deisseroth K 2011 *Neuron* **71** 9
[8] Nagel G, Szellas T, Huhn W, Kateriya S, Adeishvili N, Berthold P, Ollig D, Hegemann P and Bamberg E 2003 *Proc. Natl. Acad. Sci. USA* **100** 13940
[9] Boyden E S, Zhang F, Bamberg E, Nagel G and Deisseroth K 2005 *Nat. Neurosci.* **8** 1263
[10] Sohal V S and Huguenard J R 2003 *J. Neurosci.* **23** 8978
[11] Deisseroth K 2015 *Nat. Neurosci.* **18** 1213
[12] Krook-Magnuson E, Armstrong C, Oijala M and Soltesz I 2013 *Nat. Commun.* **4** 1376
[13] Krook-Magnuson E, Szabo G G, Armstrong C, Oijala M and Soltesz I 2014 *eNeuro* **1** 5

[14] Erofeev A, Gerasimov E, Lavrova A, Bolshakova A, Postnikov E, Bezprozvanny I and Vlasova O L 2019 *Appl. Sci.* **9** 3673
[15] Hristova K, Martinez-Gonzalez C, Watson T C, Codadu N K, Hashemi K, Kind P C, Nolan M F and Gonzalez-Sulser A 2021 *Brain* **144** 1576
[16] Che Y 2017 *Proceedings of the 8th International IEEE/EMBS Conference on Neural Engineering (NER)*, May 25–28, 2017, Shanghai, China pp. 469–472
[17] Zhang H, Shen Z, Zhao Y, Du L and Deng Z 2022 *Int. J. Mol. Sci.* **23** 13652
[18] Zhao J, Yu Y, Han F and Wang Q 2023 *Chaos* **33** 083128
[19] Andrasfalvy B K, Zemelman B V, Tang J and Vaziri A 2010 *Proc. Natl. Acad. Sci. USA* **107** 11981
[20] Hyder S K, Lazarini-Lopes W, Tobi J, Williams G, Sukharev A and Forcelli P A 2025 *Proc. Natl. Acad. Sci. USA* **122** e2419178122
[21] Pinault D 2004 *Brain Res. Rev.* **46** 1
[22] Zhang H, Zhang H, Liu S and Du L 2025 *Chin. Phys. B* **34** 120701
[23] Kim U, Sanchez-Vives M V and McCormick D A 1997 *Science* **278** 130
[24] Nanobashvili Z I, Surmava A G, Bilanishvili I G, Barbaqadze M G, Mariamidze M D and Khizanishvili N A 2012 *J. Behav. Brain Sci.* **2** 436
[25] Halassa M M, Siegle J H, Ritt J T, Ting J T, Feng G and Moore C I 2011 *Nat. Neurosci.* **14** 1118
[26] Paz J T, Davidson T J, Frechette E S, Delord B, Parada I, Peng K, Deisseroth K and Huguenard J R 2013 *Nat. Neurosci.* **16** 64
[27] Chang W J, Chang W P and Shyu B C 2017 *Mol. Brain* **10** 42
[28] Wicker E and Forcelli P A 2021 *Epilepsia* **62** 2283
[29] Wilson H R and Cowan J D 1972 *Biophys. J.* **12** 1
[30] Wilson H R and Cowan J D 1973 *Kybernetik* **13** 55
[31] Brunel N 2000 *J. Comput. Neurosci.* **8** 183
[32] Nikolic K, Grossman N, Grubb M S, Burrone J, Toumazou C and Degenaar P 2009 *Photochem. Photobiol.* **85** 400
[33] Stefanescu R A, Shivakeshavan R, Khargonekar P P and Talathi S S 2013 *Bull. Math. Biol.* **75** 2208
[34] Selvaraj P, Sleigh J W, Kirsch H E and Szeri A J 2016 *Phys. Rev. E* **93** 012416
[35] Williams J C, Xu J, Lu Z, Klimas A, Chen X, Ambrosi C M, Cohen I S and Entcheva E 2013 *PLoS Comput. Biol.* **9** e1003220
[36] Bansal H, Pyari G and Roy S 2023 *Photonics* **10** 501
[37] Gradinaru V, Thompson K, Zhang F, Mogri M, Kay K, Schneider M B and Deisseroth K 2007 *J. Neurosci.* **27** 14231
[38] Xu Z, Wang Y, Chen B, Xu C, Wu X, Wang Y, Zhang S, Hu W, Wang S, Guo Y, *et al*. 2016 *EBioMedicine* **14** 148
[39] Shiri Z, Manseau F, Lévesque M, Williams S and Avoli M 2016 *Ann. Neurol.* **79** 354
[40] Ladas T P, Chiang C C, Gonzalez-Reyes L E, Nowak T and Durand D M 2015 *Exp. Neurol.* **269** 120
[41] Pinault D and Deschenes M 1992 *Neuroscience* **51** 259
[42] Sohal V S, Zhang F, Yizhar O and Deisseroth K 2009 *Nature* **459** 698
[43] Wang L, Xu W, Wang K, Yang J, Li H, Wang Q, Dong Z, Zhang X, Meng Q, Lu F, *et al*. 2025 *Nat. Commun.* **16** 9228
[44] Cotic M, Chinvarun Y, Guirgis M, Carlen P L and Bardakjian B L 2014 *Proceedings of the* 36*th Annual International Conference of the IEEE Engineering in Medicine and Biology Society, August 26–30, 2014, Chicago, IL, USA* pp. 4455–4458
[45] Gradinaru V, Mogri M, Thompson K R, Henderson J M and Deisseroth K 2009 *Science* **324** 354